Journal of Magnetic Resonance 204 (2010) 340–345

Contents lists available at ScienceDirect

Journal of Magnetic Resonance

journal homepage: www.elsevier.com/locate/jmr

Communication

In vivo application of sub-second spiral chemical shift imaging (CSI) to hyperpolarized ^{13}C metabolic imaging: Comparison with phase-encoded CSI

Dirk Mayer [a,b,*], Yi-Fen Yen [c], Yakir S. Levin [a], James Tropp [d], Adolf Pfefferbaum [b,e], Ralph E. Hurd [c], Daniel M. Spielman [a]

[a] Stanford University, Department of Radiology, Richard M. Lucas Center for Imaging, 1201 Welch Rd., Stanford, CA 94305, United States
[b] SRI International, Neuroscience Program, 333 Ravenswood Ave., Menlo Park, CA 94025, United States
[c] GE Healthcare, 333 Ravenswood Ave., Menlo Park, CA 94025, United States
[d] GE Healthcare, 47697 Westinghouse Drive, Fremont, CA 94539, United States
[e] Stanford University, Department of Psychiatry and Behavioral Sciences, 401 Quarry Rd., Stanford, CA 94305, United States

ARTICLE INFO

Article history:
Received 14 September 2009
Revised 4 March 2010
Available online 9 March 2010

Keywords:
Hyperpolarized metabolic imaging
^{13}C
Dynamic nuclear polarization
Pyruvate
Rat

ABSTRACT

A fast spiral chemical shift imaging (CSI) has been developed to address the challenge of the limited acquisition window in hyperpolarized ^{13}C metabolic imaging. The sequence exploits the sparsity of the spectra and prior knowledge of resonance frequencies to reduce the measurement time by undersampling the data in the spectral domain. As a consequence, multiple reconstructions are necessary for any given data set as only frequency components within a selected bandwidth are reconstructed "in-focus" while components outside that band are severely blurred ("spectral tomosynthesis"). A variable-flip-angle scheme was used for optimal use of the longitudinal magnetization. The sequence was applied to sub-second metabolic imaging of the rat *in vivo* after injection of hyperpolarized [1-^{13}C]-pyruvate on a clinical 3T MR scanner. The comparison with conventional CSI based on phase encoding showed similar signal-to-noise ratio (SNR) and spatial resolution in metabolic maps for the substrate and its metabolic products lactate, alanine, and bicarbonate, despite a 50-fold reduction in scan time for the spiral CSI acquisition. The presented results demonstrate that dramatic reductions in scan time are feasible in hyperpolarized ^{13}C metabolic imaging without a penalty in SNR or spatial resolution.

1. Introduction

The recent development of metabolic imaging of hyperpolarized ^{13}C-labeled compounds [1–3] presents new opportunities for the *in vivo* investigation of metabolism under normal and pathologic conditions. One of the technical challenges is the limited time available for imaging before the hyperpolarized signal has decayed to thermal equilibrium levels. Therefore, fast chemical shift imaging (CSI) methods are desirable, and several techniques have been developed recently for application to metabolic imaging of hyperpolarized substrates [4–14]. Hu et al. [12] exploited the sparse spectra, which occur in metabolic imaging of hyperpolarized [1-^{13}C]-pyruvate, by applying compressed sensing [15] to speed up the acquisition or increase the spatial resolution. An alternative strategy for exploiting spectral sparsity is undersampled spiral CSI [6,8]. Whereas spiral CSI (spCSI) [16] potentially allows the acquisition of an entire slice with a single excitation, multiple excitations are necessary for most applications to achieve the necessary spectral bandwidth (SW) due to limitations in gradient hardware. This is especially the case for ^{13}C-CSI because the lower gyromagnetic ratio corresponds to a fourfold decrease in gradient performance compared to proton MRI. However, the number of spatial interleaves can be reduced significantly by undersampling in the spectral dimension. Because the enhanced longitudinal magnetization is not replenished between excitations, a reduction in scan time does not necessarily lead to a loss in signal-to-noise ratio (SNR) in hyperpolarized MRI [17,18]. Golman and Petersson [2] have compared the gold-standard free induction decay CSI (FIDCSI) based on phase encoding (PE) with a multi-echo steady-state free-precision technique [4] and found similar metabolite distributions with comparable SNR but at higher spatial resolution. Yen et al. [14] evaluated how excitation flip angle and phase encoding schemes affect SNR and point spread function (PSF) of FIDCSI. The aim of this work was to compare sub-second undersampled spCSI to FIDCSI and demonstrate that dramatic reductions in scan time are feasible in hyperpolarized ^{13}C metabolic imaging without the penalty in SNR or spatial resolution that occurs in CSI performed using thermal equilibrium polarization levels.

* Corresponding author. Address: Stanford University, Richard M. Lucas Center for Imaging, Department of Radiology, 1201 Welch Road, Stanford, CA 94305-5488, United States. Fax: +1 650 723 5795.
E-mail addresses: dirk.mayer@stanford.edu, dirk.mayer@sri.com (D. Mayer).

1090-7807/$ - see front matter © 2010 Elsevier Inc. All rights reserved.
doi:10.1016/j.jmr.2010.03.005

2. Material and methods

2.1. CSI acquisition parameters

We compared 3-shot spCSI with phase-encoded FIDCSI using a field of view (FOV) of 80 × 80 mm^2 with a nominal in-plane resolution of 5 × 5 mm^2. In both sequences, a 1.8-ms minimum phase radio frequency (RF) pulse (2289-Hz bandwidth) was used for slice selection in superior/inferior (S/I) direction. For each of the three spiral interleaves, 32 gradient echoes were acquired at a 250-kHz readout bandwidth with an interval of 3.6 ms corresponding to a SW of 276.2 Hz and nominal spectral resolution of 8.6 Hz. A variable-flip-angle (VFA) scheme was applied for the three excitations to compensate for the loss of longitudinal magnetization due to RF depletion. The excitation flip angle was progressively increased as $\theta_i = \mathrm{atan}(1/\sqrt{n_{tot}-i})$ [19] with $n_{tot} = 3$ and $1 \leqslant i \leqslant n_{tot}$. With a repetition time (TR) of 125 ms, the total acquisition time per slice was 375 ms.

The VFA scheme with $n_{tot} = 256$ was also used for the comparative FIDCSI acquisition where it was combined with a centric PE order [3], i.e., the order of the PE steps is based on the distance from the *k*-space center with the center being acquired first. It has been shown that this acquisition strategy reduces image blurring while maintaining high SNR [14]. As the full square *k*-space area was sampled, the nominal point spread function was slightly narrower compared to spCSI when using the same spatial apodization (a full width at half maximum (FWHM) of 7.2 mm compared to 8.5 mm). For each phase encoding step, 256 data points were acquired at a SW of 5000 Hz corresponding to a nominal spectral resolution of 19.5 Hz. With a TR of 75 ms, the total acquisition time was 19.2 s.

2.2. Polarization procedure and animal handling

Substrate, polarization procedure, and animal handling were the same as described in [8]. A final liquid-state polarization of (23.6 ± 0.8)% (mean ± s.d., $n = 4$) was achieved using a HyperSense system (Oxford Instruments Molecular Biotools, Oxford, UK). For *in vivo* experiments, 3.2 mL of the final 80-mM pyruvate solution with a pH of 7.35 ± 0.06 were injected manually into a healthy male Wistar rat (409 g body weight) through a tail vein catheter at a rate of approximately 0.2 mL/s. For phantom experiments, the concentration of the hyperpolarized pyruvate solution was 19 mM. All procedures were approved by the Institutional Animal Care and Use Committees at Stanford University and SRI International.

2.3. MR protocol

The experiments were performed on a clinical 3T Signa MR scanner (GE Healthcare, Waukesha, WI) equipped with self-shielded gradients (40 mT/m, 150 mT/m/ms). A custom-built dual-tuned (^{1}H/^{13}C) quadrature rat coil (inner diameter: 80 mm, length: 90 mm), operating at 127.7 MHz and 32.1 MHz, respectively, was used for both RF excitation and signal reception. The coil was based on a previously published design [20] with a second half-Helmholtz unit added to provide quadrature operation in the proton mode.

Single-shot fast spin-echo proton MR images in axial, sagittal, and coronal orientations were repeatedly acquired throughout the scanning session as anatomical references for prescribing the ^{13}C-CSI experiments. In each direction, up to 45 2-mm slices were acquired with 0-mm separation and a nominal in-plane resolution of 0.47 mm (256 × 192 matrix, echo time (TE)/TR = 38.6/1492 ms).

The transmit ^{13}C RF power was calibrated and the CSI sequences were tested using a reference phantom containing an 8-M solution of ^{13}C-urea in 80:20 w/w water:glycerol and 3 μL/mL Gd-chelate (OmniScan™, GE Healthcare, Oslo), which was placed on top of the animal. The phantom was also used as a concentration reference to normalize the metabolic images. It was removed prior to the first spCSI measurement because the aliased urea resonance at 163.5 ppm would partially overlap with the pyruvate signal.

Four injections of hyperpolarized [1-^{13}C]-pyruvate were performed at an interval of approximately 2 h, each one followed by a CSI acquisition (alternating FIDCSI and spCSI: FID1, sp1, FID2, sp2) from a 10-mm slice through the right kidney of the animal. Probably due to intestinal movements, the position of the kidney had shifted through the course of the experiment by a few mm, so that the prescriptions for the second and third/fourth CSI scans were adjusted accordingly to center the slice on the organ. The delay between start of injection and start of CSI acquisition was 20 s. A single data set was acquired for each FIDCSI acquisition, whereas four spCSI acquisitions were performed at an interval of 10 s to take advantage of spins flowing into the slice after the first acquisition.

For phantom experiments, a 10-mm slice from a syringe (12-mm inner diameter) filled with 3.6 mL of hyperpolarized pyruvate was measured. The time delay between dissolution and start of acquisition was 45 s.

2.4. Data processing and analysis

All data processing was performed with custom software using Matlab (MathWorks Inc., Natick, MA). Because of the short acquisition time per PE step of only 51.2 ms, the FIDCSI data were strongly apodized in the time dimension with a 20-Hz Gaussian line broadening and zero-filled by a factor of 8. In the spatial frequency dimensions the data were apodized by a generalized Hamming window ($\alpha_{apo} = 0.7$) and zero-filled by a factor of 4. After performing a 3D fast Fourier transform (FFT), the data were corrected for frequency shifts due to B_0 inhomogeneity using the dominant pyruvate signal. Metabolic images were calculated by peak integration (in absorption mode) with the baseline estimated by a straight line through the spectral points at the beginning and end of the integration interval. Phase-correction was done for each resonance separately by multiplying the spectrum in each voxel with a constant phase so that the respective peak would appear in absorption mode. The integration interval was determined by the peak width in a spectrum from a kidney voxel and was 64 Hz for pyruvate (Pyr), lactate (Lac), and alanine (Ala), and 52 Hz for bicarbonate (Bic).

The spCSI data from the first three time points (20 s, 30 s, and 40 s after start of injection) were evaluated for the comparison as they cover approximately the same time interval as the duration of the FIDCSI acquisition. The data from these three time points were reconstructed as described in [8], first individually and a second time when added together. An additional phase correction step was added to the reconstruction to reduce localization artifacts caused by phase differences between the acquisitions for the three interleaves. For each spiral gradient echo, the phase at the center of *k*-space was calculated as the average of data points 5–10. After subtracting the phase of the first interleaf from the other two interleaves, a linear component along the spiral gradient echoes was estimated for the phase difference for interleaves 2 and 3 and then subtracted from the respective interleaf (cf. Suppl. Fig. 1). Because of the higher nominal spectral resolution, the data were apodized with a 5-Hz Gaussian line broadening. Metabolic images were calculated in the same way as for the FIDCSI data. However, due to the higher spectral resolution the integration interval was 28 Hz for Pyr, Lac, and Ala, and 22 Hz for Bic.

The metabolic images were normalized to the signal intensity of the 8-M urea phantom at thermal equilibrium (polarization of

2.64×10^{-4}%) acquired with the respective sequence and using the same post-processing parameters as for the metabolites. For better comparison, the intensity values for each acquisition were also corrected for the amount of polarization at the time of dissolution, i.e., scaled to the average polarization of the four dissolutions. As there is still uncertainty regarding the *in vivo* values of the metabolite T_1s, the intensities are expressed in units of mM $\times$ % polarization (mM%). In this notation the urea phantom has an intensity of 2.1 mM%. Note also that the time delays from dissolution to start of injection and to start of data acquisition were the same for all CSI measurements, so that the SNR comparison is not affected by the value of T_1.

Whereas the noise level in MRS is usually estimated by the standard deviation of the signal in a spectral region that contains no resonances, this is not applicable in the case of undersampled spCSI due to the proximity of the metabolite peaks. Therefore, the noise level for both CSI techniques was estimated in each metabolic image by the standard deviation of the intensity in a 375-mm^2 region (a total of 300 pixels) outside the animal. Hence, this quantity is also affected by any signal artifacts due to imperfect localization.

3. Results and discussion

To illustrate the effect of aliasing in undersampled spCSI, Fig. 1a–d shows spectra of Pyr, Lac, Ala, and Bic from the same voxel in the center of the right kidney acquired with 3-shot spCSI after the fourth injection. For each spectrum, the reconstruction bandwidth was chosen so that the respective resonance was "in-focus". For comparison, Fig. 1e shows a spectrum from the same voxel acquired with FIDCSI after the third injection. Note that a manual first-order phase correction was performed for the FIDCSI spectrum and the baseline was subtracted by fitting a spline to signal-free regions of the smoothed spectrum. Although the metabolite signals cover a spectral range of more than 700 Hz at 3T, the resonances of Pyr and its metabolic products were still well separated when using spCSI with a SW of only 276 Hz. Only the signal from [1-^{13}C]-pyruvate hydrate (Pyh) could not be resolved from Pyr. However, pyruvate hydrate is in dynamic equilibrium with pyruvate (<8%) and is itself not metabolically active [1]. Therefore, it has only minor effects on the quantitation of Pyr.

Fig. 2 compares the metabolic images of the four metabolites from all four CSI measurements. In case of spCSI, only the data acquired at 20 s after start of injection are shown. Despite a more than 50-fold increase in imaging speed, the images acquired with spCSI show similar localization quality and SNR as the FIDCSI images. The biggest differences in image quality between the two CSI techniques are seen in the Bic images. This is to be expected, as it is the smallest signal and closest to the dominant Pyr peak. The two resonances are only 40 Hz apart due to the spectral aliasing. To compare the spatial resolution of the methods, Fig. 3 shows cross-sections through the metabolic images for both Pyr and Lac from the third and fourth CSI experiment (FID2 and sp2). The cross-sections were taken through the image center along both the anterior/posterior (A/P) and right/left (R/L) directions. Although the nominal PSF for FIDCSI was narrower than for spCSI, the cross-sections in Fig. 3a and b indicate a stronger blurring in the FIDCSI image of Pyr compared to spCSI. As the start of acquisition was approximately 4 s after the injection had been finished, the reduction of Pyr signal during the 20-s acquisition both through longitudinal relaxation and metabolic conversion lead to an additional weighting of the data acquired at the outer *k*-space

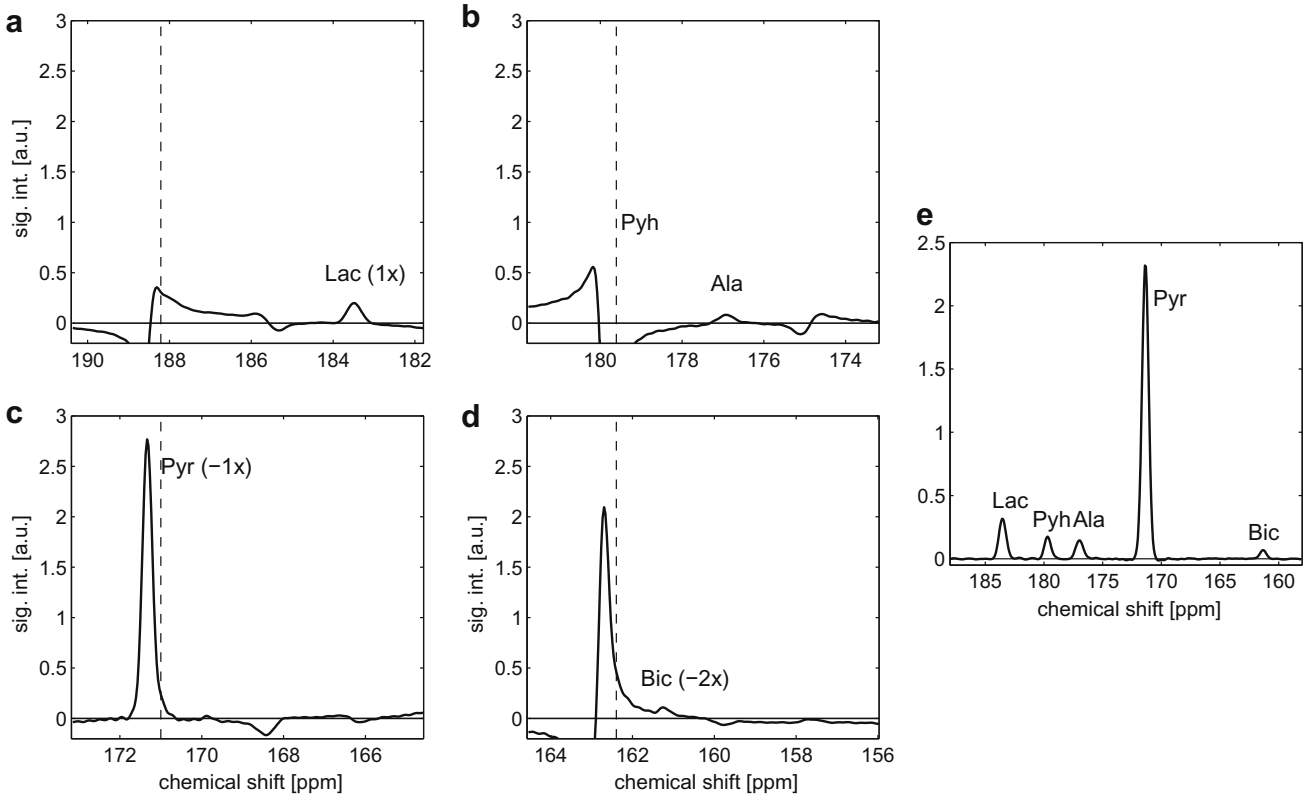

Fig. 1. Single spectra acquired with spCSI in 375 ms (a–d) from a voxel (interpolated nominal size: 1.25 $\times$ 1.25 $\times$ 10 mm^3) at the center of the right kidney. In undersampled spCSI, separate reconstructions have to be performed for resonances that have been aliased. At the chosen center frequency and a SW of 276.2 Hz, Lac (a) was aliased once, Ala (b) was not aliased, Pyr (c) was aliased once, and Bic (d) was aliased twice. The vertical dashed lines indicate the frequency of Pyh. Only a 0th order phase correction was applied to put the respective resonance in absorption mode. (e) Corresponding spectrum acquired with FIDCSI in 19 s. Both 0th and 1st order phase corrections were applied and the baseline subtracted.

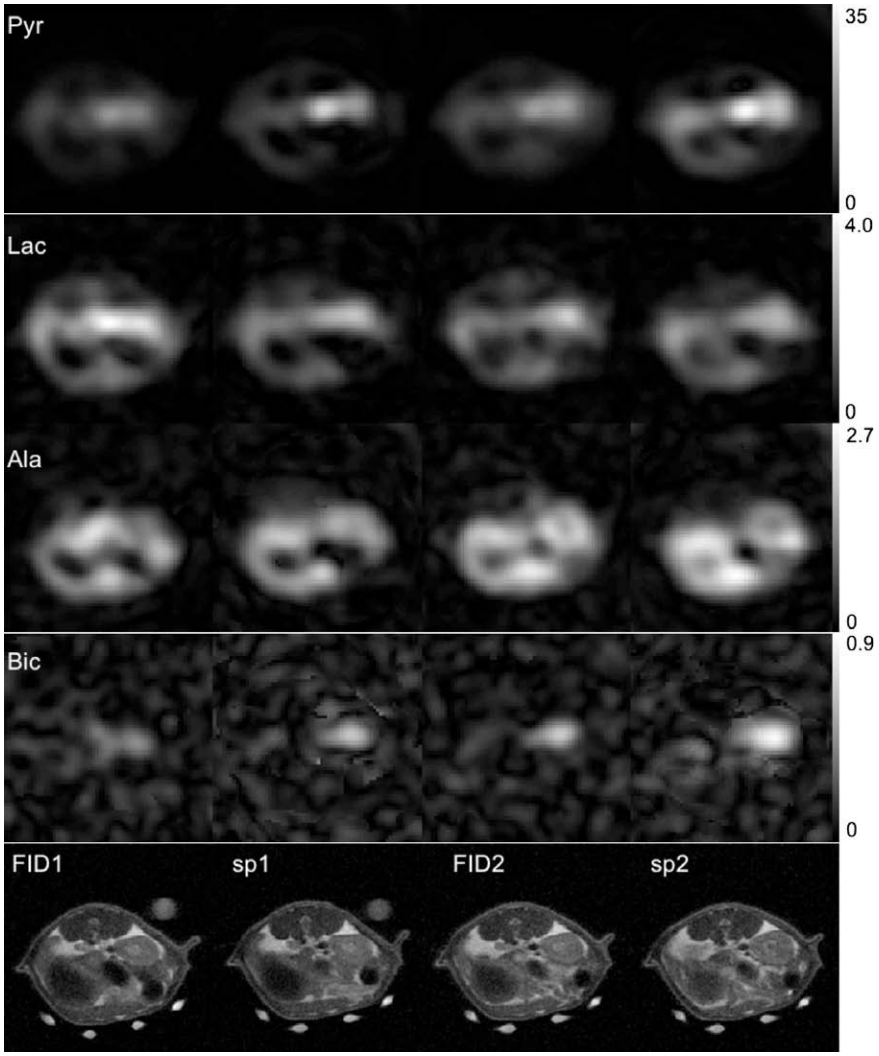

Fig. 2. Metabolic images of Pyr (top row), Lac (2nd row), Ala (3rd row), and Bic (4th row) from the four CSI acquisitions. The image intensities are in units of mM% and normalized to the average polarization level from the four dissolutions. The corresponding ^{1}H MRI are shown in the bottom row.

regions with the applied PE scheme. This has also been shown by Yen et al. [14] by simulating the FIDCSI sequence and using measured dynamic data. During the 375-ms duration of spCSI, the signal variations have a considerably smaller effect. Comparing the cross-sections for Lac (Fig. 3c and d) suggests similar spatial resolution for the two techniques as the signal decay due to T_1 relaxation during the 20-s FIDCSI acquisition was partially compensated by additional Lac, which was produced by conversion from Pyr. The spatial resolution was also compared in a cylindrical phantom filled with hyperpolarized pyruvate. Cross-sections along R/L and A/P directions through the center of the phantom are shown in Fig. 4. The FWHM was 10.8 mm for spCSI and 11.9 mm for FIDCSI. Simulating the two pulse sequences for a disc with a 12-mm diameter and a T_1 of 60 s results in a FWHM of 10.9 mm for spCSI and 11.1 mm for FIDCSI. The relatively large difference for FIDCSI is likely due to deviations from the ideal flip angle scheme. For this pulse sequence, calibrating excitation B_1 too high leads to a faster depletion of the longitudinal magnetization that results in additional apodization of the k-space data. A miscalibration of the RF has less of an effect on the spatial resolution in spCSI as the center of k-space is sampled in all interleaves and can be used to correct for this.

For a quantitative comparison, Table 1 contains average image intensity and SNR values from all four *in vivo* CSI acquisitions measured in an ROI of 6×6 voxels (interpolated nominal size: $7.5 \times 7.5 \times 10\ \mathrm{mm}^3$) in the center of the right kidney. Also listed are the corresponding values for spCSI when the acquisitions at 20 s, 30 s, and 40 s were added together ($\mathrm{sp1}_{\mathrm{sum}}$ and $\mathrm{sp2}_{\mathrm{sum}}$). SNR values are reported as SNR in the respective image, as SNR normalized to mean polarization (nSNR), and as SNR with the noise level taken from an image of the urea phantom prior to the injection ($\mathrm{nSNR}_{\mathrm{ref}}$). In the case of the summed spCSI data, the noise level from the urea image was multiplied by $\sqrt{3}$. The largest variations in intensity are found for Pyr. Considering the different dynamics of the metabolites, e.g., see Fig. 1 in [14], Pyr is the most sensitive to the timing of the acquisition relative to the bolus injection. This is probably also the reason for the large difference between Pyr measured with FIDCSI and with spCSI when comparing the mean metabolite values for the two methods. The relative differences for Bic are likely due to the low SNR. Although it cannot be ruled out that differences in metabolite concentrations were due to physiological effects of multiple injections, pyruvate metabolism appears to be rapid and no cumulative effect is expected at imaging intervals of 1.5 h [14]. The data from the sum of the three spCSI acquisitions indicate considerable in-flow effects for both substrate and products. For the products, the additional signal could be from conversion of "fresh" Pyr in the kidney or products flowing into the imaging slice after being produced elsewhere in the body. On average for all four metabolites, spCSI yields very similar SNR values as FIDCSI despite the 50-fold reduction in acquisition time.

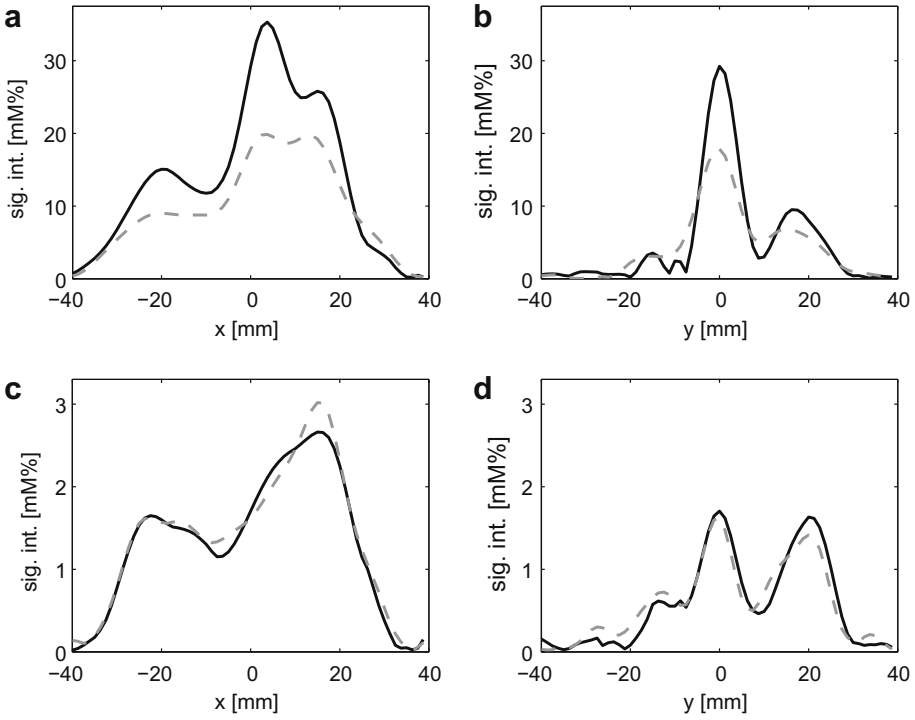

Fig. 3. Cross-sections along R/L direction through the center of the metabolic images for Pyr (a) and Lac (c) acquired with spCSI (solid black) and FIDCSI (dashed grey). (b) and (d), same as (a) and (c) but along A/P direction.

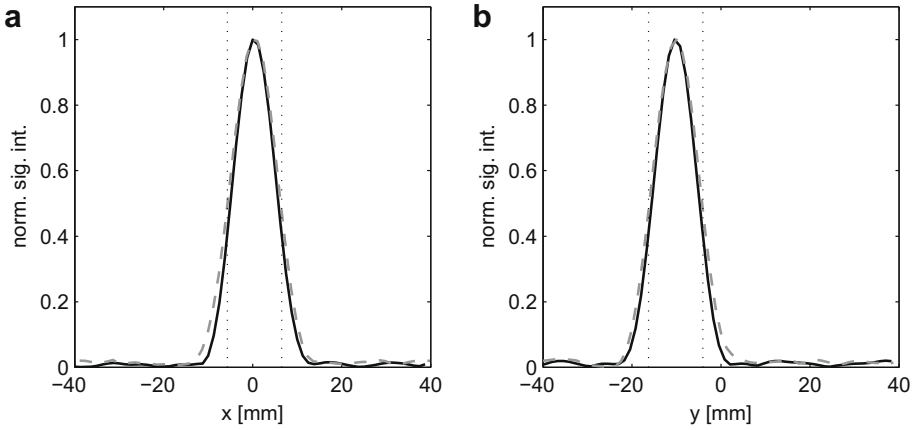

Fig. 4. Cross-sections along R/L (a) and A/P (b) directions through the center of a cylindrical phantom filled with a solution of hyperpolarized [1-^{13}C]-pyruvate, acquired with spCSI (solid black) and FIDCSI (dashed grey).

Table 1
Signal intensity and SNR values of the four metabolites from an ROI in the center of the right kidney. SNR denotes the SNR in the respective image (as described in data analysis), nSNR is the SNR corrected for polarization (normalized to the average polarization for the four dissolutions), and $nSNR_{ref}$ the polarization-corrected SNR with the noise level measured in a metabolic image of the reference urea phantom.

	FID1	FID2	sp1	sp2	$sp1_{sum}$	$sp2_{sum}$	FID1	FID2	sp1	sp2	$sp1_{sum}$	$sp2_{sum}$
	Pyr						*Lac*					
Sig. (mM%)	14.0	18.0	16.5	23.9	22.3	29.1	3.1	2.4	2.5	2.4	4.4	4.5
SNR	76	79	70	110	72	89	45	44	39	53	45	49
nSNR	80	76	70	108	73	87	47	42	39	52	46	48
$nSNR_{ref}$	346	442	326	473	232	332	75	60	49	48	50	51
	Ala						*Bic*					
Sig. (mM%)	1.1	1.6	1.4	1.4	2.3	2.3	0.5	0.5	0.5	0.8	0.9	1.1
SNR	18	24	27	24	25	16	13	13	13	17	14	20
nSNR	19	23	27	24	25	16	14	12	13	17	14	20
$nSNR_{ref}$	27	39	28	27	27	27	9	11	10	15	10	13

However, it is interesting that for both techniques much higher SNR values were found when the noise level from the urea reference image was used for the SNR calculation. This is in particular the case for Pyr, indicating that for high-SNR metabolic imaging the SNR is dominated by signal artifacts arising from imperfect localization. Potential causes for the localization artifacts are change in longitudinal magnetization and concentration during the acquisition, animal motion during acquisition, Gibbs ringing, and, in case of spCSI, deviation between theoretical and actual *k*-space trajectory. The latter can be corrected by using the measured trajectory in the gridding reconstruction.

4. Conclusion

The presented data demonstrate that hyperpolarized ^{13}C *in vivo* metabolic imaging with a total acquisition time of 375 ms is feasible using undersampled spiral CSI on a clinical 3T scanner. The comparison with conventional CSI using phase encoding shows similar resolution and SNR. Unlike with *in vivo* CSI performed using thermal equilibrium polarization levels, the reduction in acquisition time in hyperpolarized metabolic imaging does not lead to a reduction in SNR proportional to the square root of acquisition time. The shorter acquisition time can be used to extend the spatial coverage (see Supplementary Fig. 2 for metabolic images from a multi-slice experiment in which 11 slices were acquired in 4.1 s) and for dynamic metabolic imaging with high temporal resolution [8]. The shorter acquisition time is also advantageous when imaging potential hyperpolarized compounds with shorter T_1. Due to the FID acquisition mode, quantitation is hampered by a non-constant phase of the resonances leading to baseline distortions. This is particularly a problem in undersampled spCSI due to the spectral aliasing that reduces spectral separation between signals and introduces additional phase distortions from "out-of-focus" components. One possibility to improve quantitation is using a dual spin-echo with full echo acquisition mode [9]. This allows quantitation in magnitude mode without introducing line broadening, hence, eliminating the problem of baseline distortions due to out-of-phase components. Further improvement can potentially be achieved by using prior knowledge, e.g. resonance frequencies, scalar coupling constants, transverse relaxation times, line widths, and B_0 field maps, and estimating the amplitudes with a minimum least-squares solution [7,10]. Due to the limitation of the clinical gradient system, multiple spatial interleaves were still necessary to achieve a sufficient spectral bandwidth. However, single-shot metabolic imaging should be possible when using a high-performance gradient insert [21].

Acknowledgments

We thank Oliver Hsu, B.A., and Evan Nunez, B.A., for assistance in animal handling and monitoring. This study was supported by the Lucas Foundation and National Institutes of Health Grants RR09784, AA05965, AA13521-INIA, CA114747, and EB009070.

Appendix A. Supplementary material

Supplementary data associated with this article can be found, in the online version, at doi:10.1016/j.jmr.2010.03.005.

References

[1] K. Golman, R. In't Zandt, M. Thaning, Real-time metabolic imaging, Proc. Natl. Acad. Sci. USA 103 (2006) 11270–12705.
[2] K. Golman, J.S. Petersson, Metabolic imaging and other applications of hyperpolarized 13C1, Acad. Radiol. 13 (2006) 932–942.
[3] S.J. Kohler, Y. Yen, J. Wolber, A.P. Chen, M.J. Albers, R. Bok, V. Zhang, J. Tropp, S. Nelson, D.B. Vigneron, J. Kurhanewicz, R.E. Hurd, In vivo 13 carbon metabolic imaging at 3T with hyperpolarized 13C-1-pyruvate, Magn. Reson. Med. 58 (2007) 65–69.
[4] S. Månsson, J. Leupold, O. Wieben, R. In't Zandt, P. Magnusson, E. Johansson, J. Petersson, Metabolic imaging with hyperpolarized 13C and multi-echo, single-shot RARE, in: Proceedings of the 14th Annual Meeting of the ISMRM, Seattle, WA, 2006, p. 584.
[5] J. Leupold, S. Mansson, J.S. Petersson, J. Hennig, O. Wieben, Fast multiecho balanced SSFP metabolite mapping of (1)H and hyperpolarized (13)C compounds, Magma 22 (2009) 251–256.
[6] D. Mayer, Y.S. Levin, R.E. Hurd, G.H. Glover, D.M. Spielman, Fast metabolic imaging of systems with sparse spectra: application for hyperpolarized 13C imaging, Magn. Reson. Med. 56 (2006) 932–937.
[7] Y.S. Levin, D. Mayer, Y.F. Yen, R.E. Hurd, D.M. Spielman, Optimization of fast spiral chemical shift imaging using least squares reconstruction: application for hyperpolarized (13)C metabolic imaging, Magn. Reson. Med. 58 (2007) 245–252.
[8] D. Mayer, Y.F. Yen, J. Tropp, A. Pfefferbaum, R.E. Hurd, D.M. Spielman, Application of subsecond spiral chemical shift imaging to real-time multislice metabolic imaging of the rat in vivo after injection of hyperpolarized 13C1-pyruvate, Magn. Reson. Med. 62 (2009) 557–564.
[9] C.H. Cunningham, A.P. Chen, M.J. Albers, J. Kurhanewicz, R.E. Hurd, Y.F. Yen, J.M. Pauly, S.J. Nelson, D.B. Vigneron, Double spin-echo sequence for rapid spectroscopic imaging of hyperpolarized 13C, J. Magn. Reson. 187 (2007) 357–362.
[10] S.B. Reeder, J.H. Brittain, T.M. Grist, Y.F. Yen, Least-squares chemical shift separation for 13C metabolic imaging, J. Magn. Reson. Imaging 26 (2007) 1145–1152.
[11] W.H. Perman, P. Bhattacharya, A.P. Lin, J.B. Hovener, K.C. Harris, E.Y. Chekmenev, V.A. Norton, D.P. Weitekamp, B.D. Ross, Fast spatial–spectral imaging of hyperpolarized 13C compounds using partial-Fourier multipleecho 3DFIESTA, in: Proceedings of the 15th Annual Meeting of the ISMRM, Berlin, Germany, 2007, p. 1250.
[12] S. Hu, M. Lustig, A.P. Chen, J. Crane, A. Kerr, D.A. Kelley, R. Hurd, J. Kurhanewicz, S.J. Nelson, J.M. Pauly, D.B. Vigneron, Compressed sensing for resolution enhancement of hyperpolarized (13)C flyback 3D-MRSI, J. Magn. Reson. 192 (2008) 258–264.
[13] P.E. Larson, A.B. Kerr, A.P. Chen, M.S. Lustig, M.L. Zierhut, S. Hu, C.H. Cunningham, J.M. Pauly, J. Kurhanewicz, D.B. Vigneron, Multiband excitation pulses for hyperpolarized 13C dynamic chemical-shift imaging, J. Magn. Reson. 194 (2008) 121–127.
[14] Y.F. Yen, S.J. Kohler, A.P. Chen, J. Tropp, R. Bok, J. Wolber, M.J. Albers, K.A. Gram, M.L. Zierhut, I. Park, V. Zhang, S. Hu, S.J. Nelson, D.B. Vigneron, J. Kurhanewicz, H.A. Dirven, R.E. Hurd, Imaging considerations for in vivo 13C metabolic mapping using hyperpolarized 13C-pyruvate, Magn. Reson. Med. 62 (2009) 1–10.
[15] M. Lustig, D. Donoho, J.M. Pauly, Sparse MRI: the application of compressed sensing for rapid MR imaging, Magn. Reson. Med. 58 (2007) 1182–1195.
[16] E. Adalsteinsson, P. Irarrazabal, S. Topp, C. Meyer, A. Macovski, D.M. Spielman, Volumetric spectroscopic imaging with spiral-based k-space trajectories, Magn. Reson. Med. 39 (1998) 889–898.
[17] J.P. Mugler III, J.R. Brookeman, Signal-to-noise considerations for parallel imaging with hyperpolarized gases, in: Proceedings of the 13th Annual Meeting of the ISMRM, Miami, FL, 2005, p. 485.
[18] R. Lee, G. Johnson, C. Stefanescu, R. Trampel, G. McGuinness, B. Stoeckel, A 24-ch phased-array system for hyperpolarized helium gas parallel MRI to evaluate lung functions, Conf. Proc. IEEE Eng. Med. Biol. Soc. 4 (2005) 4278–4281.
[19] L. Zhao, R. Mulkern, C.H. Tseng, D. Williamson, S. Patz, R. Kraft, R.L. Walsworth, F.A. Jolesz, M.S. Albert, Gradient-echo imaging considerations for hyperpolarized 129Xe MR, J. Magn. Reson. B 113 (1996) 179–183.
[20] K. Derby, J. Tropp, C. Hawryszko, Design and evaluation of a novel dual-tuned resonator for spectroscopic imaging, J. Magn. Reson. 86 (1990) 645–651.
[21] B. Chronik, A. Alejski, B.K. Rutt, Design and fabrication of a three-axis multilayer gradient coil for magnetic resonance microscopy of mice, Magma 10 (2000) 131–146.